Electronic Supplementary information (ESI)

Solvent-Free Synthesis of Renewable FDCA-based Bis-Cyclic Carbonate Using a Metal-Free Heterogeneous Catalyst

Giovanni Berluti,[a] Angelo Scopano,[a] Gabriele Galletti,[a] Edwin Otten, [b] Coralie Jehanno [c] and Paolo P. Pescarmona[a,*]

[a] *Chemical Engineering group, Engineering and Technology institute Groningen (ENTEG), University of Groningen, Nijenborgh 3, 9747 AG Groningen, The Netherlands. * Corresponding author: p.p.pescarmona@rug.nl*

[b] *Stratingh Institute for Chemistry, University of Groningen, Nijenborgh 3, 9747 AG Groningen, The Netherlands.*

[c] *POLYKEY POLYMERS, Gipuzkoa science and technology park, Miramon Pasealekua 170, 20014, Donostia-San Sebastian, Spain.*

Table of Contents

Green metrics calculation

The renewable carbon content was calculated as the bio-derived C wt.% for each furanic molecule. In this calculation, we considered methanol and allyl bromide as being of fossil origin as the massive production of this compounds it is still petroleum-derived, while glycidol and glycerol carbonate are considered as originating from renewable sources, as a relevant number of industrial routes to produce these compounds employ glycerol as a feedstock.

The atom efficiency of the synthetic routes was calculated by dividing the molecular weight of the products for the sum of the molecular weights of all reagents. For the synthesis of BDFCC starting from FDCA and GlyC, also ethyl-(N',N' dimethylamino) propylcarboimide hydrochloride was considered as a starting material as it is used stoichiometrically in the synthesis.

The occupational exposure level values are reported in terms of time-weighted average (TWA) or short-term exposure limit (STEL), and can be found searching for the international safety cards released by the international labour organisation (ILO) in collaboration with the world health organisation (WHO).[1]

Set-up configurations

Three different configurations (Fig. S1) were adopted to study the effect of by-product removal.
When a "closed vessel" condition was required, a 20 mL glass test tube was sealed using a rubber Suba-Seal septum. On the contrary, to study an "open vessel" configuration, the previous septum was not used, and the vial was left open.
When a "open vessel under N_2 flow" (gas-flow) configuration was required for the experiment, a gas line was connected to the "closed vessel" configuration, piercing the septum with a needle (0.8 mm of diameter and 120 mm of length) so that the tip of the needle was immersed into the reaction mixture. A second needle (0.8 mm of diameter and 50 mm of length) was used to pierce the septum and avoid the pressure build-up. The gas flow rate was controlled by a Bronkhorst mass flow controller previously calibrated for each gas using a bubble gas-flow reader.

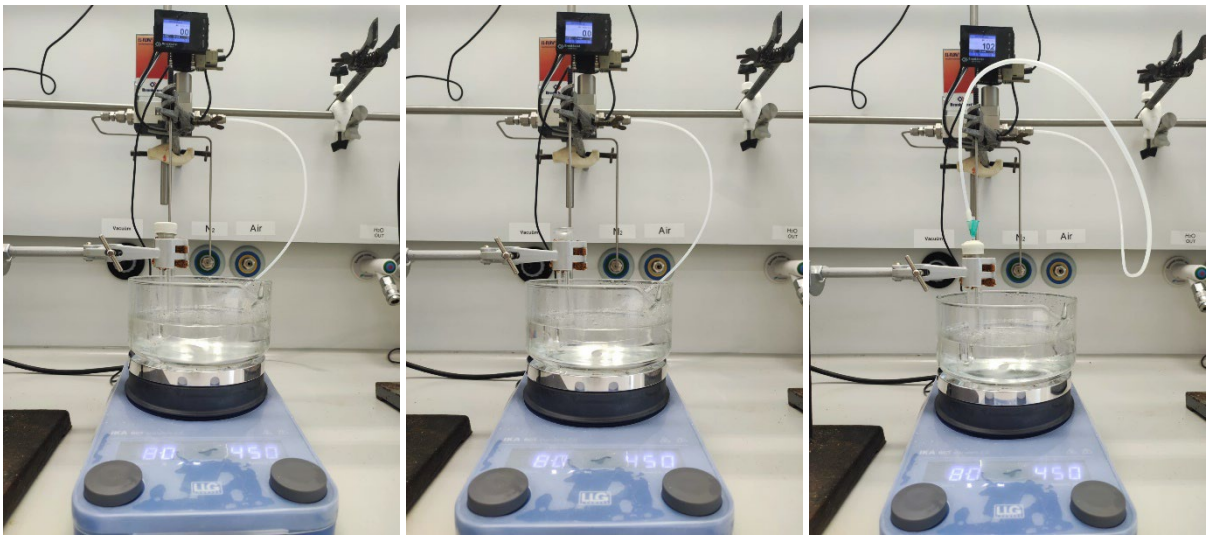

Figure S1 Set-up configurations adopted in this work (from left to right): closed, open and open vessel under N_2 flow.

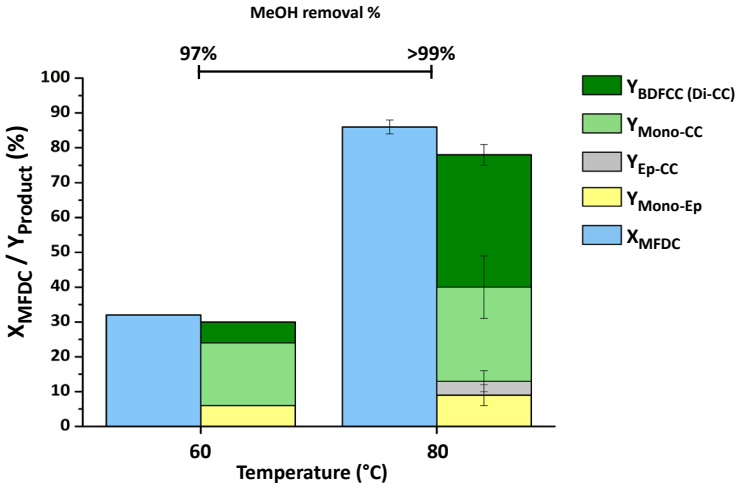

Figure S2 Effect of the reaction temperature (60 or 80 °C) using the open vessel configuration under N_2 flow. Conditions: MFDC (1 mmol), GlyC (2.2 mmol), Amb IRA-900-Cl (30 mg), Gly (0.4 mmol), no solvent, 7 h, 10 ml min^{-1} of N_2. The test at 80 °C was performed in triplicate.

DFT calculations

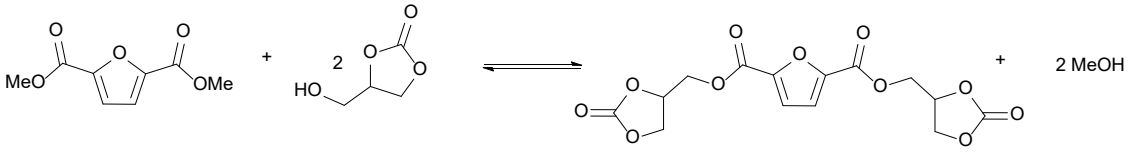

Figure S3 Reaction scheme for which the Gibbs free energy was calculated.

The Gibbs free energy of MFDC, Glycerol carbonate, BDFCC and methanol were calculated using Gaussian 16, Revision B.01. The data resulting from the different calculation are hereby reported in Tables S1, S2 and S3.

Table S1 Thermodynamic parameters calculated using the Gaussian 16 program by geometry and frequencies optimisation using the B3LYP/ def2TZVP method in the gas-phase at 298K. ε_0 : electronic energies, H_{corr} : thermal correction for enthalpy, G_{corr} : thermal correction for the Gibbs free energy. a: conformer of MFDC and BDFCC depicted in Fig. S4.

Molecule	ε_0 (E_h)	H_{Corr}	G_{Corr}	$\Delta_rG^0_{(1)}$ (kJ mol^{-1})	$\Delta_rH^0_{(1)}$ (kJ mol^{-1})	$\Delta_rS^0_{(1)}$ (kJ mol^{-1} K^{-1})
MFDC[a]	-686.06	0.168861	0.114866			
GlyC	-457.127	0.115994	0.075648	+40	+40	-0.00025
MeOH	-115.776	0.289576	0.209046			
BDFCC[a]	-1368.75	0.055324	0.02826			

Table S2 Thermodynamic parameters calculated using the Gaussian 16 program by geometry and frequencies optimisation using the B3LYP/def2TZVP method and including Grimme's D3 dispersion in the gas-phase at 298 K. a, b: conformers of MFDC and BDFCC depicted in Fig. S4.

Molecule	ε_0 (E_h)	H_{Corr}	G_{Corr}	$\Delta_rG^0_{(2a)}$ (kJ mol^{-1})	$\Delta_rH^0_{(2a)}$ (kJ mol^{-1})	$\Delta_rS^0_{(2a)}$ (kJ mol^{-1} K^{-1})	$\Delta_rG^0_{(2b)}$ (kJ mol^{-1})	$\Delta_rH^0_{(2b)}$ (kJ mol^{-1})	$\Delta_rS^0_{(2b)}$ (kJ mol^{-1} K^{-1})
MFDC[a]	-686.074	0.1688	0.1149						
MFDC[b]	-686.075	0.1688	0.1150						
GlyC	-457.137	0.1160	0.0757	+29	+26	-0.013	+27	+23	-0.014
MeOH	-115.777	0.0553	0.0282						
BDFCC[a]	-1368.784	0.2900	0.2108						
BDFCC[b]	-1368.786	0.2900	0.2109						

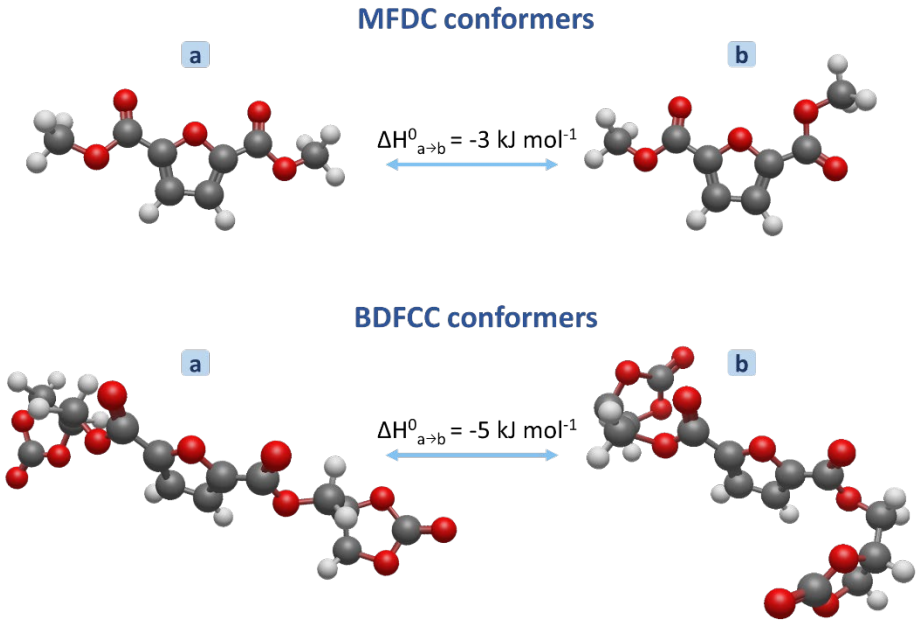

Figure S4 Initial geometries of possible MFDC and BDFCC conformations and related energy differences.

Table S3 Thermodynamic parameters calculated using the Gaussian 16 program by single point analysis using the B3LYP/ def2TZVP method, including Grimme's D3 dispersion and SMD method using DMSO at 298 K.

Molecule	ε_0 (E_h)	$\Delta rE_{solv}{}^0_{(3b)}$ (kJ mol^{-1})	$\Delta_rG^0_{(2b)}$ (kJ mol^{-1})	$\Delta_rG^0_{(3b)}$ (kJ mol^{-1})
MFDC[b]	-686.0897			
GlyC	-457.1547	-1.95	+27	+25
MeOH	-1368.8281			
BDFCC[b]	-115.7811			

The thermodynamic parameters reported in Tables S1, S2 and S3 were calculated as follows:
Equations 1 and 2 were used to calculate the enthalpy and the Gibbs free energy (in kJ mol^{-1}) of each molecule in the gas phase at 298 K.
Equations 1[a] and 2[a] were used to calculate the enthalpy and Gibbs free energy of reaction at 298.15 K.
Equation 3 was used to calculate the entropy difference of the target transesterification at 298.15 K. Equation 4 was used to calculate the Gibbs free energy at 353.15 K assuming enthalpy and entropy being independent of temperature.

Eq. 1 $$H\ (kJ\ mol^{-1}) = E_0 + H_{corr} \times 627.5 \times 4.184$$

Eq. 2 $$G\ (kJ\ mol^{-1}) = E_0 + G_{corr} \times 627.5 \times 4.184$$

Eq. 1[a] $$\Delta_r H^0_{298.15K}\ (kJ\ mol^{-1}) = \sum \nu\ H_{products} - \sum \nu\ H_{reagents}$$

Eq. 2[a] $$\Delta_r G^0_{298.15K}\ (kJ\ mol^{-1}) = \sum \nu\ G_{products} - \sum \nu\ G_{reagents}$$

Eq. 3 $$\Delta_r S^0_{298.15K}\ (kJ\ mol^{-1}\ K^{-1}) = (\Delta_r H^0_{298.15K} - \Delta_r G^0_{298.15K})/T$$

Eq. 4 $$\Delta_r G_{353.15K}\ (kJ\ mol^{-1}) = \Delta_r H^0_{298.15K} - 353.15 \times \Delta_r S^0_{298.15K}$$

After calculation of the Gibbs free energy, the equilibrium constant (K_{eq}) was determined using equation 5.

Eq. 5 $$\Delta_r G_{353.15K}(kJ\ mol^{-1}) = -8.314 \times 10^{-3} \times 353.15 \times \ln K_{eq}$$

Once the equilibrium constant was determined, the "Solver" function of the Microsoft Excel program was used to calculate the equilibrium concentration of BDFCC ($C_{BDFCC(Eq.)}$) by subjecting as a constrain the equivalence between the Gaussian calculated K_{eq} and the one calculated by the solver.

$$K_{eq} = \frac{C_{BDFCC(Eq.)} \times {C_{MeOH(Eq.)}}^2}{C_{FDME(Eq.)} \times {C_{GlyC(Eq.)}}^2} = \frac{4x^3}{(C_{FDME(t0)} - x) \times (C_{GlyC(t0)} - 2x)^2}$$

Finally, knowing the equilibrium concentration of each species involved, the equilibrium conversion for the target transesterification was calculated using the formula:

$$X_{FDME(Eq.)} = \frac{C_{MFDC(t0)} - C_{MFDC(Eq.)}}{C_{MFDC(t0)}} \times 100\%$$

The Gibbs free energy of the optimised geometries considering the solvation energy of DMSO at 298.15 K was calculated using equation 6:

Eq. 6 $$\Delta_r G^0_{DMSO,298.15K} = \Delta_r G^0_{gas,298.15K} + (\Delta E_{solvation})$$

where $\Delta r G^0_{gas,298.15K}$ is the Gibbs free energy difference of the reaction at the optimised geometry and $\Delta E_{solvation}$ is the difference in electronic energy between the solvated system considering DMSO and the one of the optimised geometries in gas-phase. The final Gibbs free energy at 353.15K was then calculated using equation 5. For the calculation of the reverse reaction, the same procedure was adopted using the Excel Solver for the reverse Gibbs free energy calculated in DMSO.

Table S4. Gibbs free energy, equilibrium constant and equilibrium conversion calculated based on the thermodynamic data reported in Tables S1, S2 and S3.

$\Delta_r G_{(1),353.15K}$ (kJ mol^{-1})	+40
$K_{(1)eq,353.15K}$	1.20E-06
$X_{(1)eq,353.15K}$	1.1%
$\Delta_r G_{(2a),353.15K}$ (kJ mol^{-1})	+30
$K_{(2a)eq,353.15K}$	3.64E-05
$X_{(2a)eq,353.15K}$	3.2%
$\Delta_r G_{(2b),353.15K}$ (kJ mol^{-1})	+28
$K_{(2b)eq,353.15K}$	7.19E-05
$X_{(2b)eq,353.15K}$	4.0%
$\Delta_r G_{(3a),353.15K}$ (kJ mol^{-1})	+26
$K_{(3a)eq,353.15K}$	1.46E-04
$X_{(3a)eq,353.15K}$	5.0%
$\Delta_r G_{(3b),353.15K}$ (kJ mol^{-1})	-26
$K_{(3b)eq,353.15K}$	6.9E+03
$X_{(3b)eq,353.15K}$	95.0 %

The thermodynamic parameters calculated with the Gaussian program were compared to the experimental results obtained performing the reverse reaction of methanolysis of BDFCC. This test was performed adding to a 20 mL glass test tube, BDFCC (1 mmol, previously synthetised in this work), methanol (2 mmol), Amberlite IRA-900-Cl (16 wt.% relative to BDFCC), glycidol (40 mol% relative to BDFCC) and 1 mL of DMSO used as a model solvent. The test was performed in a closed vessel configuration, heated at 80 °C (353.15 K) and stirred at 450 rpm. The conversion of BDFCC was measured by collecting samples for ^{1}H-NMR analysis over time. The reaction reached an equilibrium conversion of BDFCC of 89 % after 21 h, maintaining a constant value afterwards (88 % at 92 h, Fig. S5).

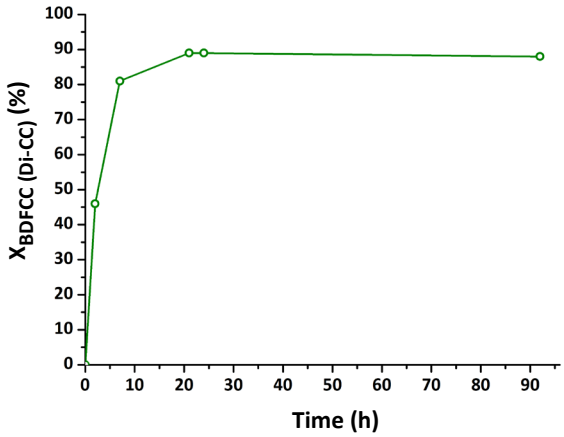

Figure S5 Conversion rate of the reverse reaction of methanolysis of BDFCC to glycerol carbonate and MFDC.

Catalyst recyclability test

The recyclability test was performed in a 20 mL glass test tube provided of magnetic stirrer and heated in an oil bath. MFDC (1 mmol), Amb IRA-900-Cl (16 wt.% relative to MFDC), glycerol carbonate (10 mmol) and glycidol (40 mol% relative to MFDC) were added in this order. A N_2-gas flow of 30 mL min^{-1} was adopted using the previously described "open vessel under N_2 flow" configuration. The reaction was left stirring at 80 °C and 450 rpm using a 10 x 3 mm magnetic rod instead of the usual 10 x 6 mm counterpart to avoid mechanical friction that could have led to the embrittlement of the Amberlite beads over multiple runs.
In the last two runs of this test, the product yields (Y) and MFDC conversion (X) were normalised (*) by the mole balance (MB) as follows:

$$Y_{product} : MB = Y^*_{product} : 100$$

$$X^*_{MFDC} = 1 - \frac{C_{f,MFDC}}{C_{0,MFDC}} \times \frac{100}{MB}$$

Table S5. Normalised values of run 4 and 5 of the recyclability test. The results are reported in %.

	X_{MFDC}	$Y_{Mono\text{-}CC}$	$Y_{BDFCC\ (Di\text{-}CC)}$	$Y_{Mono\text{-}Ep}$	$Y_{Ep\text{-}CC}$	MB%
Run 4	86	29	34	7	18	102
Run 5	86	25	37	15	18	109
			Normalised values			
Run 4	86	28	33	7	17	100
Run 5	87	22	34	14	17	100

The recyclability test procedure was repeated to study the effect of reintroducing glycidol. However, the test was stopped after the second run, as it was found that without glycidol no detectable yield of furanic functionalised cyclic carbonates were achieved (Fig. S6).

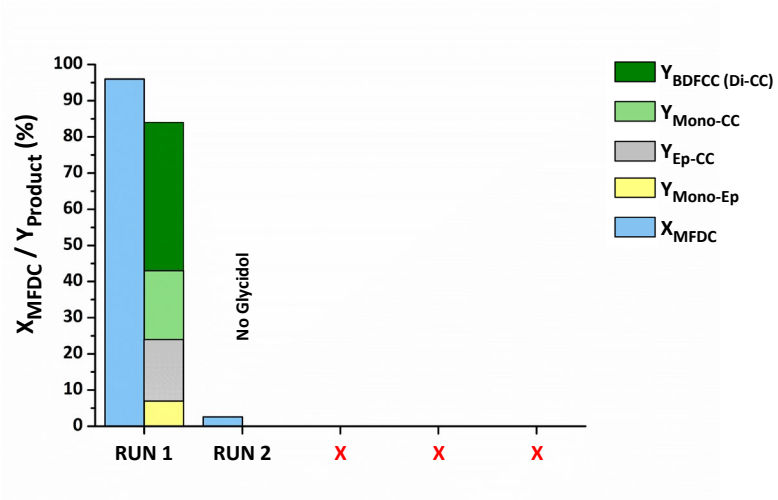

Figure S6 Recyclability test without glycidol. Same reaction conditions reported in Figure 7, but without glycidol reintroduction.

Synthesis of BDFCC

Table S6 Mono-Ep and Ep-CC side-products formation over time. Conditions reported in Figure 2 a-b (Entries 1-2) and Figure 6 a-b (Entries 3-4). *: averaged values of the different replicates.

Entry	Ratio (GlyC : MFDC)	$Y_{Mono\text{-}Ep}$			$Y_{Ep\text{-}CC}$		
		2h	7h	24h	2h	7h	24h
1	2.2 : 1	11*	13*	6*	2*	4*	8*
2	2.2 : 1	9*	9*	4*	6*	4*	4*
3	4.4 : 1	11	8	1	0	6	8
4	10 : 1	15	0	0	0	0	0

Up-scaled synthesis configuration

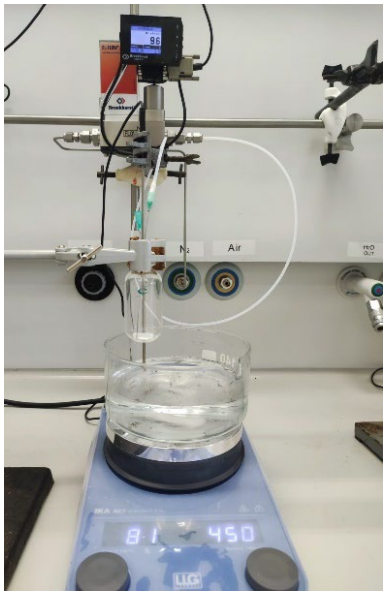

Figure S7 Up-scaled gas-flow configuration.

The 20-times scaled-up transesterification of MFDC with GlyC was performed using a gas-flow system with a 73 mL min^{-1} N_2 flow. In a 50 mL glass vial, MFDC (0.02 mol), GlyC (0.2 mol), Amb IRA-900-Cl (0.6 g) and Gly (0.008 mol) were added in this order. The glass vial was heated up in an oil bath at 80 °C and magnetically stirred at 450 rpm.
The 40-fold scaled-up transesterification was performed in a 100 mL round bottom flask (Fig. S8), employing 0.04 mol of MFDC while keeping the same ratio of reactants and catalyst as in the 20-times scaled-up synthesis, but using a flow of Ar instead of N_2.

Understanding the contribution of the components of the catalytic system

The Cl^- loading of the Amberlite resins used in this work is assumed to be equal to 3.83 $mmol_{Cl^-}\ g_{cat}{}^{-1}$. This value is the result of a previous study performed by our group using ionic liquid (IL) chromatography to determine the total chloride content of the beads.[2]

Table S7 Optimisation of the loading of glycidol.

Entry	Gly (% mol)	IRA-900-Cl (mg)	Ratio Gly : Cl^-
1	40	30	3.5
2	30	30	2.6
3	20	30	1.7
4	10	30	0.9
5	5	30	0.4

Table S8 Optimisation of the loading of Amberlite IRA-900-Cl.

Entry	Gly (% mol)	IRA-900-Cl (mg)	Ratio Gly : Cl^-	GlyC mole balance
1	20	70	0.7	87%
2	20	50	1.0	87%
3	20	30	1.7	87%
4	20	10	5.3	92%
5	20	5	10.5	97%

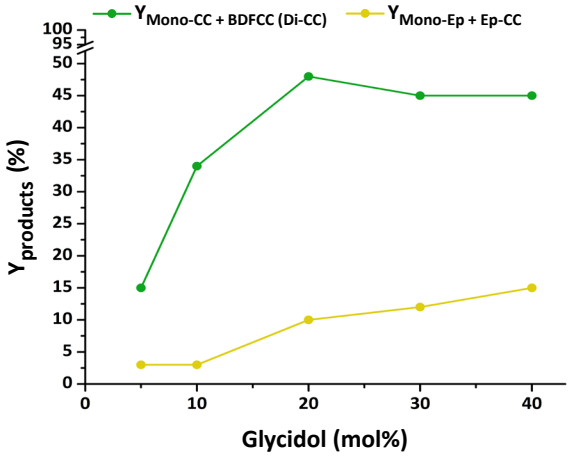

Figure S8 Selectivity towards the cyclic-carbonate-functionalised furanic products vs the epoxy-functionalised species as a function of the amount of glycidol. Same reaction conditions reported in Figure 8a.

Products identification

The main reaction products were separated by column chromatography, eluting with a mixture ethyl acetate and n-hexane (70 : 30), which was found to be the most effective mobile phase relying on the previous analysis of thin layer chromatography (TLC).

Four main fractions (FR) were separated, but not all of them resulted in a pure compound. However, since no overlap was observed for the major ^{1}H-NMR peaks, the product identification was performed without further separation steps. The products identified, listed in order of elution are: (FR1) Mono-Ep, co-eluted with MFDC (Rf: 0.04) (Fig. S9 and S10 for ^{13}C-NMR of MFDC pure); (FR2) Mono-CC (Rf: 0.18) (Fig. S11); (FR3) Ep-CC (Rf: 0.65) (Fig. S12) and (FR4) BDFCC (Rf: 0.81) (Fig. S13-S14). The last fraction (FR5) was analysed by ^{1}H-NMR to identify possible side-products. This analysis showed several compounds, among which we identified the peaks of chlorohydrin formed through the reaction between glycidol and Amberlite IRA-900-Cl (Figure S15). Quantitative ^{13}C-NMR analysis was performed on each product, to assign the peaks in the range between 145-147 ppm related to quaternary carbon of the furanic ring (Figure S16). These peaks were commonly used during the quantification to determine the ratio of the different products (see below, section on NMR quantification). Nevertheless, due to the low concentration of the purified fraction, the ^{13}C-NMR signals of the quaternary carbons on the furanic ring were less intense than usual in these spectra (compare Figures S16 and S17). However, the isolation of these products allowed us to interpret and assign the ^{1}H-NMR and ^{13}C-NMR peaks of the reaction crude (Figure S18 and 19 for the ^{1}H-NMR spectra of the reaction crude). The products Mono-CC and BDFCC were further characterised and compared to MFDC by FT-IR spectroscopy, showing for the first two products the presence of the characteristic cyclic carbonate and ester peaks at 1782 and 1719 cm^{-1}, respectively. On the contrary, in the case of MFDC only the latter peak was observed (Figure S20).

NMR quantification

The ^{1}H-NMR and ^{13}C-NMR spectra were recorded using a Bruker Advance 600 MHz NMR spectrometer. The FID data collected were elaborated using the "MestReNova" v15.0.0-34764 program.

The ^{1}H-NMR signals of the species involved in the reaction (MFDC, Mono-CC, BDFCC, Mono-Ep, and Ep-CC) significantly overlap due to their similar structure. However, it is possible to exploit the slower decay of their C nuclei to record well-separated peaks by ^{13}C-NMR spectroscopy. In this way, a robust, fast and reliable quantification method exploiting quantitative ^{13}C-NMR was developed. MFDC was used as a model compound to test NMR parameters such as the relaxation delay (D1) and the number of scans using tris (2,4-pentanedionato) chromium (III) as a relaxing agent to reduce the time of the analysis. The results of this test (Table S9) indicated that a number of scans of 256 and a D1 of 10 s is suitable to have an acceptable error (≈2%) and a moderately fast measurement (47 min). However, in some of the experiments of this work, due to the low concentration of side products detected during the analysis, the error in terms of mole balance reached 10%.

Table S9 ^{13}C-NMR spectroscopy acquisition parameters.

N° Scan	Relaxation delay D1 (s)	Average signal-to-noise ratio	Rel. Err. (%)
256	2	61	3.7
256	10	60	1.8
256	20	60	1.7

Experiment conditions: 1 mmol of MFDC, 1.8 mmol of trimethoxy benzene (internal standard) and 5 mg of tris (2,4-pentanedionato) chromium (III) (relaxing agent) were dissolved in 2.0 mL of d_6-DMSO. 0.6 - 0.7 mL of the mixture were collected for ^{13}C-NMR analysis.

Providing a reliable method to determine the ratio of the different compounds involved in the reaction, ^{13}C-NMR was used in cooperation with ^{1}H-NMR to determine the final quantification. Specifically, the carbon signals were used to determine the ratio between different species, while the ^{1}H-NMR peaks were used to define the total quantification of each compound relying on these ratios.

In a typical NMR spectroscopy analysis, the following peaks were utilised to determine the ratios BDFCC/Mono-CC and Ep-CC/Mono-CC using the ^{13}C-NMR peaks integrals. The average of the signals at 146.84 and 145.85 ppm was used for the Mono-CC; the peak at 146.29 ppm for the BDFCC and the average of the peaks at 146.92 and 145.97 ppm was used for the Ep-CC side product (Figure S17). Considering a typical ^{1}H-NMR spectrum of the reaction mixture, these three cyclic carbonates (Mono-CC, BDFCC and Ep-CC) completely overlap at 5.18, 4.65, 4.55 and 4.43 ppm (Figure S18). To assign the respective area of each product, the ^{1}H-NMR information was combined with the ^{13}C-NMR data using the following equations:

$$Mono - CC = x\ ;\ BDFCC = y\ ;\ Ep - CC = z$$

$$\frac{x}{y} = l\,\frac{z}{y} = m$$

$$K = 1x + 2y + 1z$$

$$x = \frac{K}{2l + 1 + m}$$

$$Q = 4x + 2y + 2z$$

$$x = \frac{Q}{4l + 2 + 2m}$$

where *K* and *Q* are respectively the ^{1}H-NMR areas of the peaks at 5.18 ppm (or 4.56 ppm) and 4.65 ppm while l and m are the ratios calculated using the ^{13}C-NMR areas of Mono-CC/BDFCC and Ep-CC/BDFCC, respectively. Once x is calculated, the ratios l and m are used to quantify the area of y and z. The three areas calculated for each compound at 5.18 ppm (or 4.56 ppm) and 4.65 ppm are then averaged, and the molar concentration is calculated using the area of the internal standard calculated by averaging the peaks at 6.1 and 3.7 ppm.

$$\frac{C_x}{I_x} \times N_x = \frac{C_{IS}}{I_{IS}} \times N_{IS}$$

C_x: concentration compound x
I_x: integral value of compound x
N_x: number of hydrogens related to the integral peak of compound x
Same applies for IS (internal standard)

The calculation of the Mono-Ep product is done by subtracting from the ^{1}H-NMR peaks at 4.68, 4.1, 2.85 ad 2.74 ppm the area of the Ep-CC product previously calculated. Finally, the area of the unreacted MFDC is calculated from the peaks at 7.2 ppm by subtracting the area of the Mono-CC, BDFCC (Di-CC), Mono-Ep and Ep-CC. As an additional verification step, the area of MFDC is also calculated by the ^{1}H-NMR peak at 3.8 ppm by subtracting the area of the Mono-CC and Mono-Ep products, which overlap. A different way to compare the results for MFDC is by calculating its area from the ratio between MFDC and Mono-CC at the ^{13}C-NMR spectra.

As a final countercheck, the averaged resulting areas of the different compounds were added up together and compared with the starting area resulting from the FID data. The comparison with the original peaks resulted in a relative error within ±5% in most of the cases. However, oscillations of this value were observed between experiments.
Methanol, a reaction by-product, was quantified by ^{1}H-NMR using the peak relative to the CH_3- group (3.18 ppm, d). The methanol removal extent was calculated as follows:

$$MeOH\ removal\ \% = \frac{mol_{MeOH\ theoretical} - mol_{MeOH\ reaction\ mixture}}{mol_{MeOH\ theoretical}} \times 100$$

where:

$$mol_{MeOH\ theoretical} = mol_{Mono-CC} + mol_{BFDCC} \times 2 + mol_{Mono-Ep} + mol_{Ep-CC} \times 2$$

The epoxide mole balance (Table 1) was determined by means of ^{1}H-NMR spectroscopy quantification using the same internal standard method mentioned previously (*vide supra*), by integrating the epoxide peaks and epoxy-derived species (Mono-Ep and Ep-CC) in the reaction mixture at the end of the test (3.0, 2.5 and 2.4 ppm in the case of glycidol). The final mole balance was calculated as follows:

$$Epoxide\ mole\ balance = \frac{n_{t,epoxide} + n_{t,epoxy-derived}}{n_{0,epoxide}} \times 100$$

Where $n_{t,epoxide}$ are the moles of the epoxide at the end of the test, $n_{t,epoxy-derived}$ are the summed moles of Mono-Ep and Ep-CC, and $n_{0,epoxide}$ are the moles of epoxide employed at the beginning of the test.

NMR Spectra

MFDC

^{1}H-NMR (600 MHz, d_6-DMSO) δ_H 7.44 (2H, s), 3.87 (6H, s) ppm. ^{13}C-NMR (151 MHz, d_6-DMSO) δ_C 158.32 (2C, C=O, carbonyl), 146.55 (2C, C-, furanic), 119.55 (2C, CH_3-O, esteric), 52.75 (2C, CH-, furanic) ppm. (Fig. S9-10)

Mono-Ep

^{1}H-NMR (600 MHz, d_6-DMSO) δ_H 7.49 (1H, s), 7.46 (1H, s), 4.68 (1H, d), 4.09 (1H, dd), 3.87 (3H, s), 3.33 (1H, m), 2.84 (1H, s), 2.73 (1H, s) ppm. (Fig. S9)

Mono-CC

^{1}H-NMR (600 MHz, d_6-DMSO) δ_H 7.47 (1H, s), 7.41 (1H, s), 5.17 (1H, m), 4.62 (1H, d), 4.60 (1H, d), 4.53 (1H, m), 4.40 (1H, m), 3.87 (3H, s) ppm. (Fig. S11)

Ep-CC

^{1}H-NMR (600 MHz, d_6-DMSO) δ_H 7.51 (1H, s), 7.42 (1H, s), 5.17 (1H, m), 4.68 (1H, d),4.62 (1H, d), 4.60 (1H, d), 4.53 (1H, m), 4.40 (1H, m), 4.11 (1H, dd), 3.33 (1H, m), 2.84 (1H, s), 2.73 (1H, s) ppm. (Fig. S12)

BDFCC (Di-CC)

^{1}H-NMR (600 MHz, d_6-DMSO) δ_H 7.44 (2H, s), 5.17 (2H, m), 4.62 (2H, d), 4.60 (2H, d), 4.53 (2H, m), 4.40 (2H, m) ppm. ^{13}C-NMR (151 MHz, d_6-DMSO) δ_C 157.02 (2C, C=O, ester), 155.26 (2C, C=O, cyclic carbonate), 146.26 (2C, -C=, furanic), 120.11 (CH-, furanic), 74.58 (2C, -CH-O, cyclic carbonate), 66.48 (2C, -CH_2-O, cyclic carbonate), 65.01 (2C, -CH_2-O, ester) ppm. (Fig. S13-14)

Chlorohydrin (3-Chloropropane-1,2-diol)

^{1}H-NMR (600 MHz, d_6-DMSO) δ_H 5.05 (1H, d, J= 5.3 Hz), 4.72 (1H, t, dd, J= 5.63, 5.63 Hz), 3.77 (1H, s, J= 5.68 Hz), 3.4 (4H, m) ppm. (Fig. S15)

Crude reaction mixture

^{1}H-NMR (600 MHz, d_6-DMSO) δ_H 7.51 - 7.44 (Mono-Ep + Mono-CC + BDFCC), 6.1 (IS), 5.3 (GlyC), 5.17 (Mono-CC + BDFCC), 5.06 (Chlorohydrin), 4.8 (GlyC), 4.74 (Chlorohydrin), 4.68 (Mono-Ep), 4.62 (Mono-CC + BDFCC), 4.60 (Mono-CC + BDFCC), 4.53 (Mono-CC + BDFCC), 4.5 (GlyC), 4.40 (Mono-CC + BDFCC), 4.3 (GlyC), 4.1 (MeOH + Mono-EP), 3.9 (Mono-Ep + Mono-CC + MFDC), 3.7 (IS), 3.7 (GlyC), 3.5 (GlyC), 3.18 (MeOH), 3.0 (gly), 2.84 (Mono-Ep), 2.73 (Mono-Ep), 2.5 (gly), 2.4 (gly) ppm. ^{13}C-NMR (151 MHz, d_6-DMSO) δ_C 146.95 (1C, Mono-CC), 146.5 (2C, MFDC), 146.25 (2C, BDFCC), 145.85 (1C, Mono-CC) ppm. (Fig. S17-19).

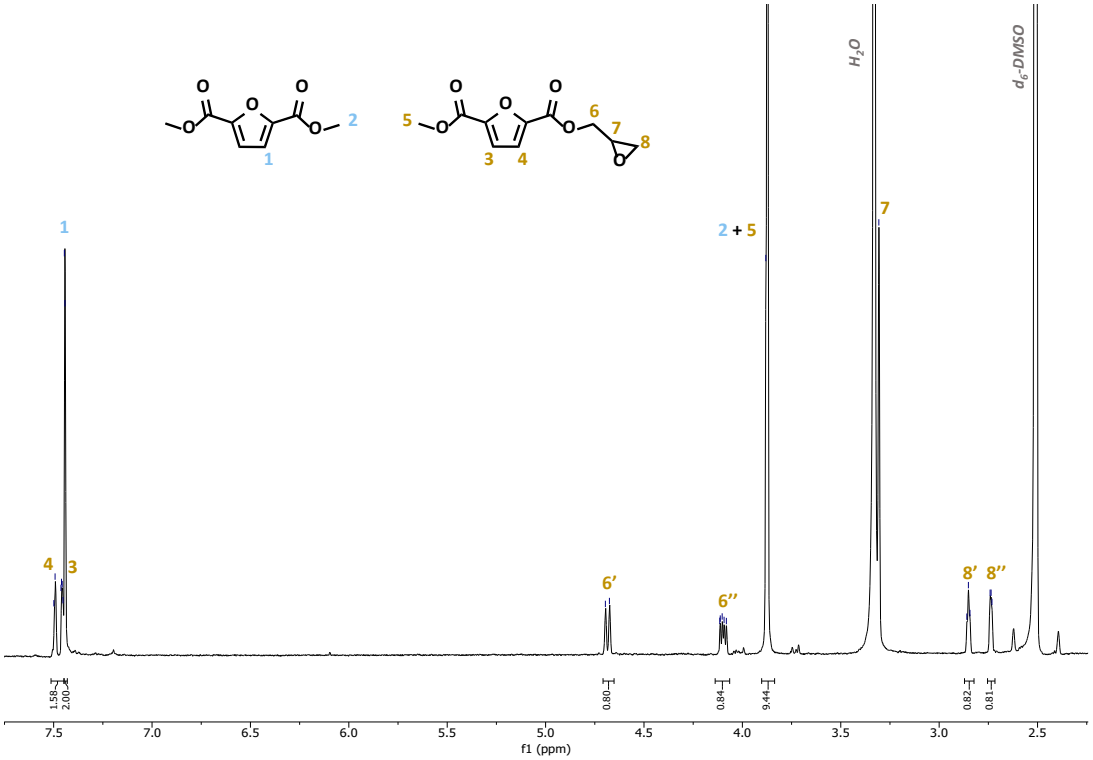

Figure S9 ^{1}H-NMR spectrum of FR1: MFDC and Mono-Ep.

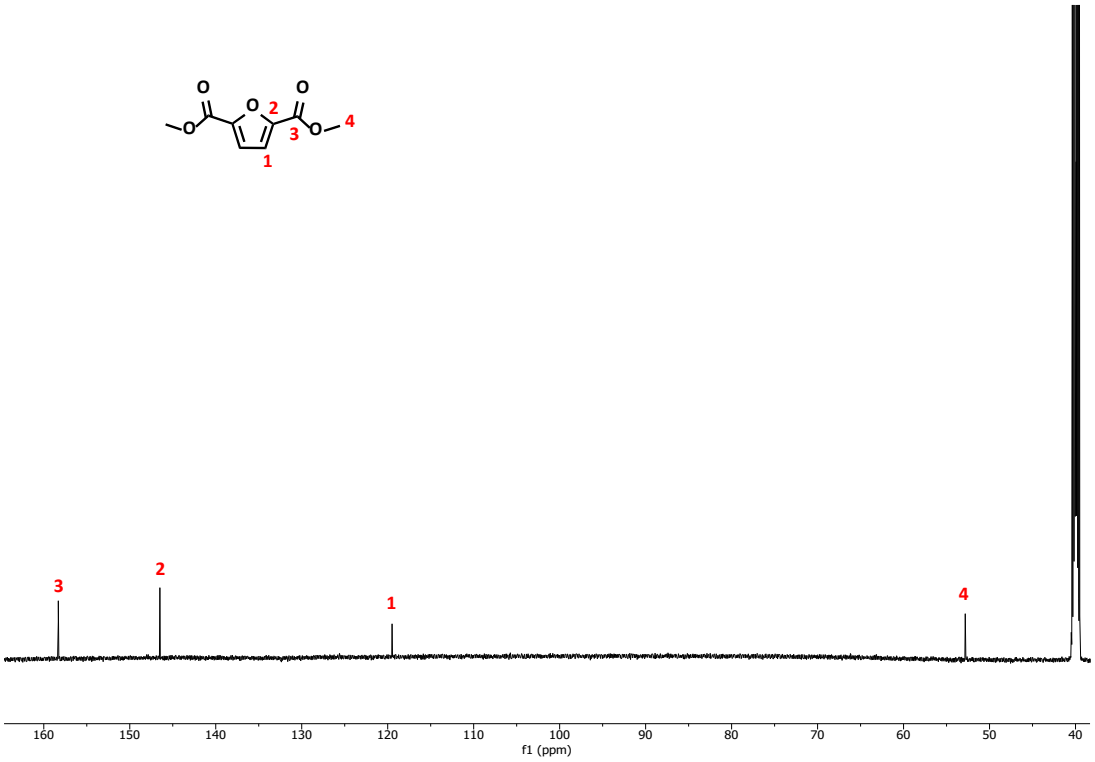

Figure S10 ^{13}C-NMR spectrum of commercial MFDC.

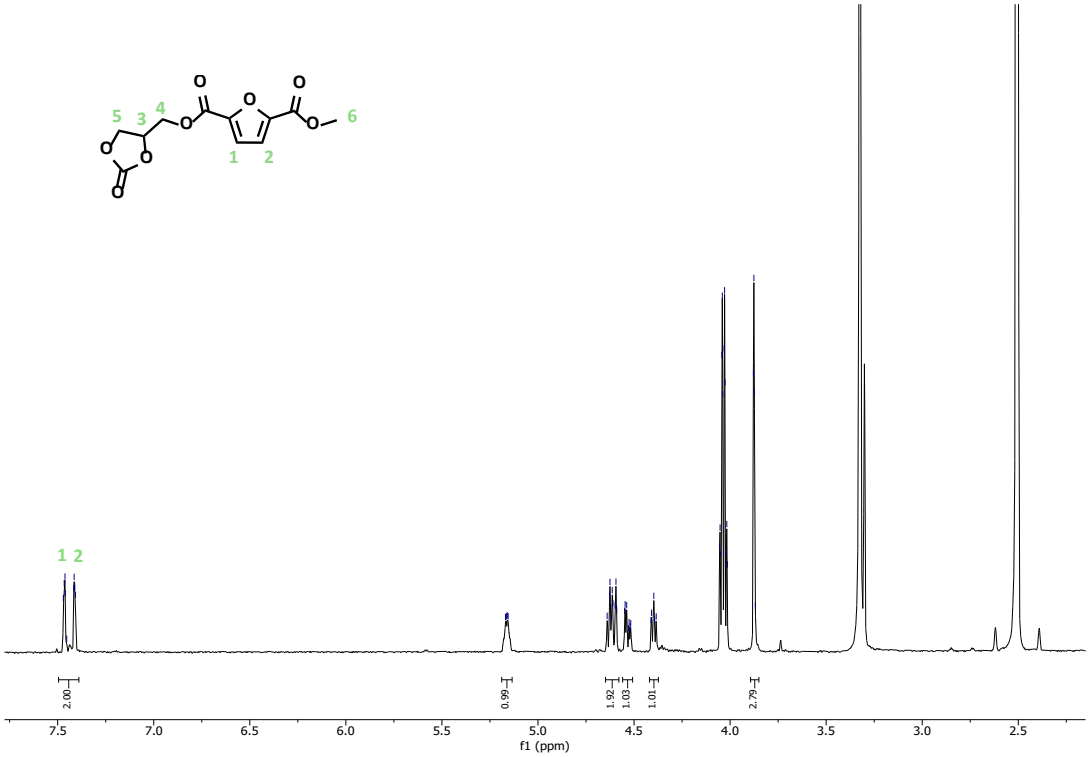

Figure S11 ^{1}H-NMR spectrum of FR2: Mono-CC.

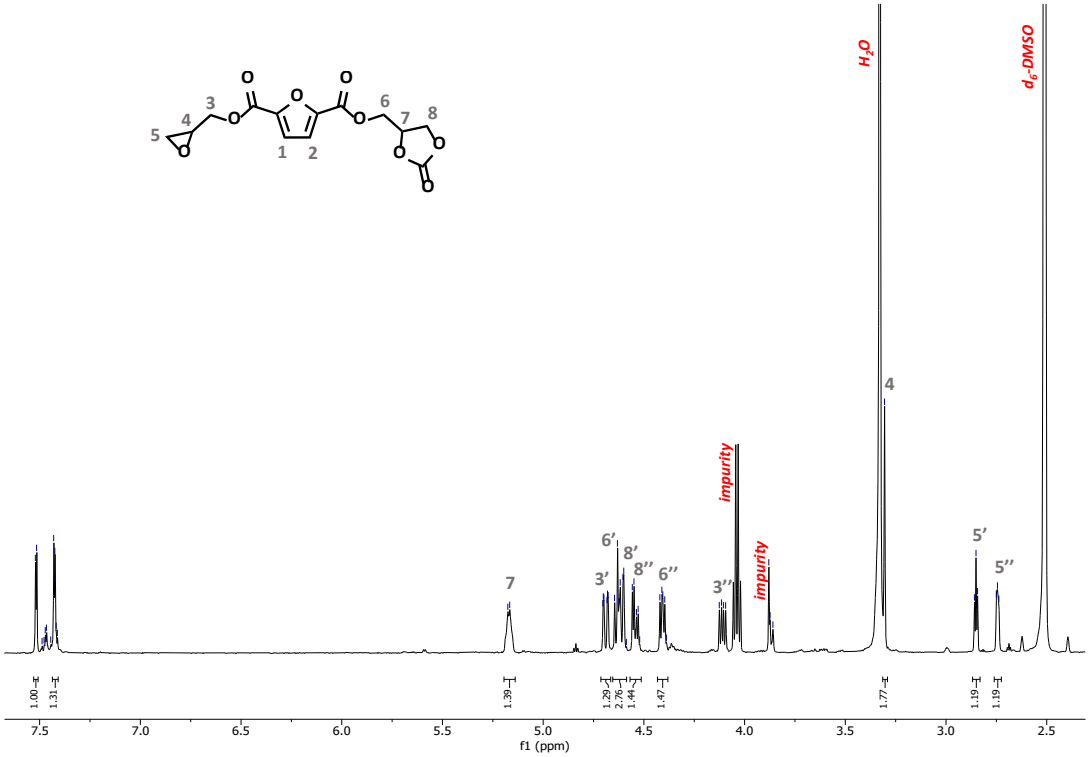

Figure S12 ^{1}H-NMR spectrum of FR3: Ep-CC.

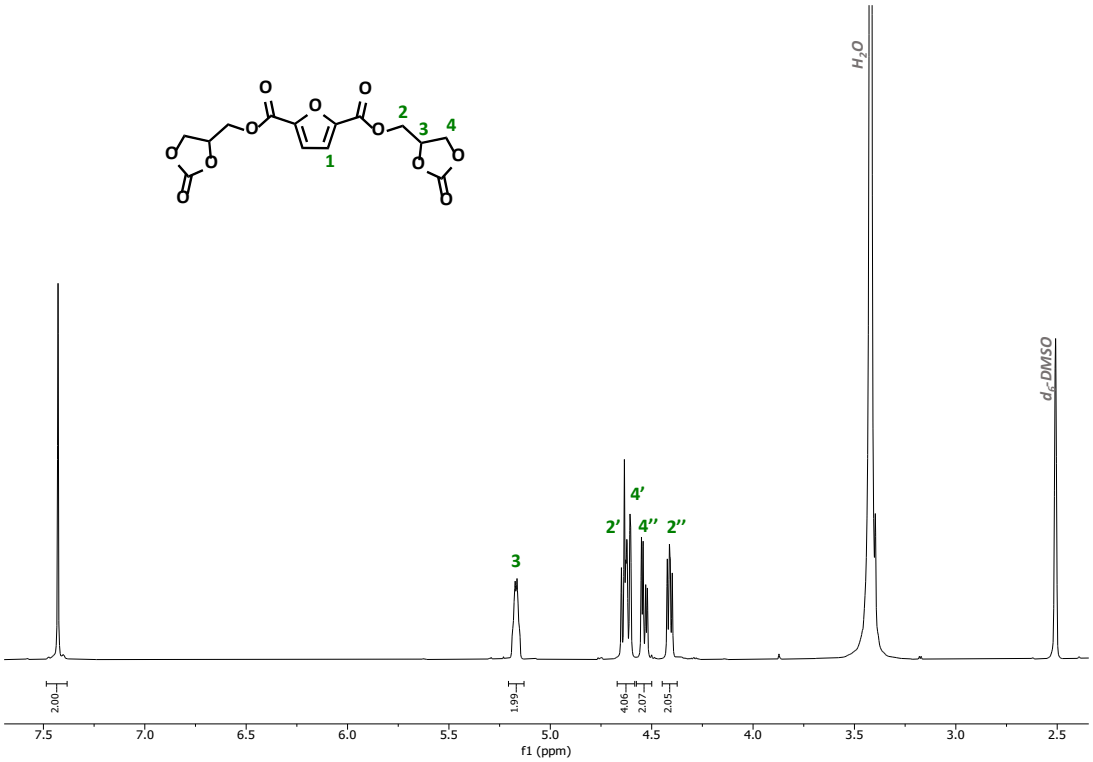

Figure S13 ^{1}H-NMR spectrum of FR4: BDFCC (Di-CC).

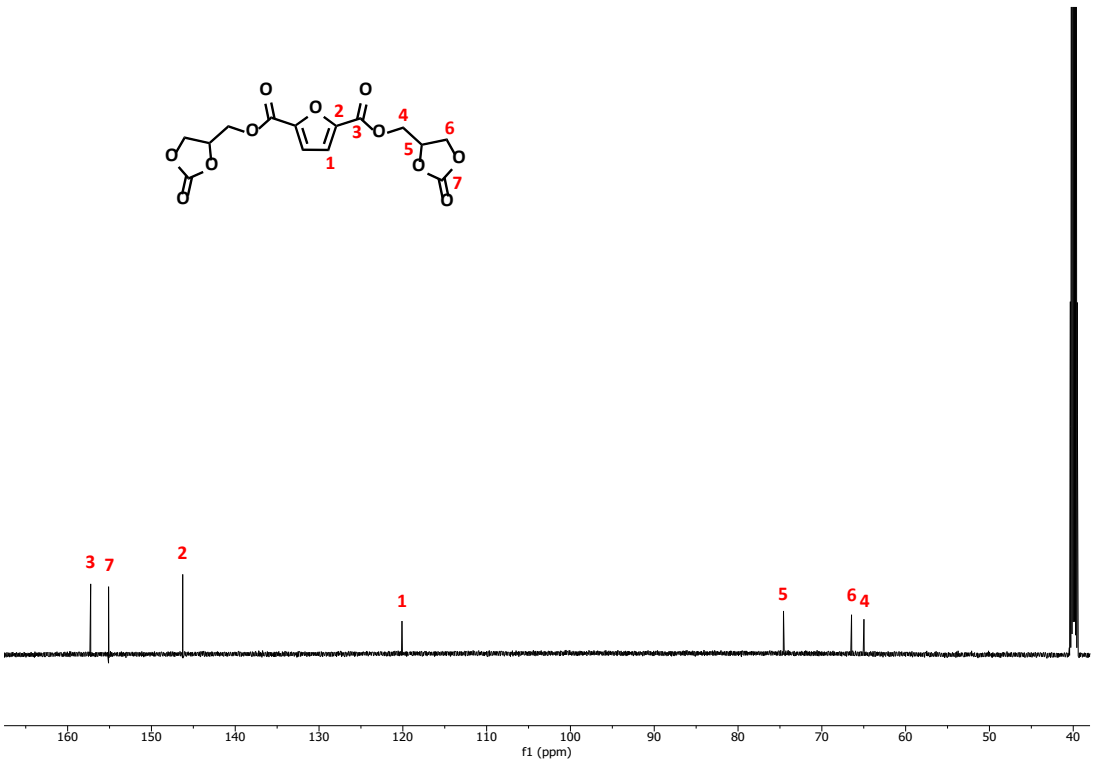

Figure S14 ^{13}C-NMR spectrum of FR4: BDFCC (Di-CC).

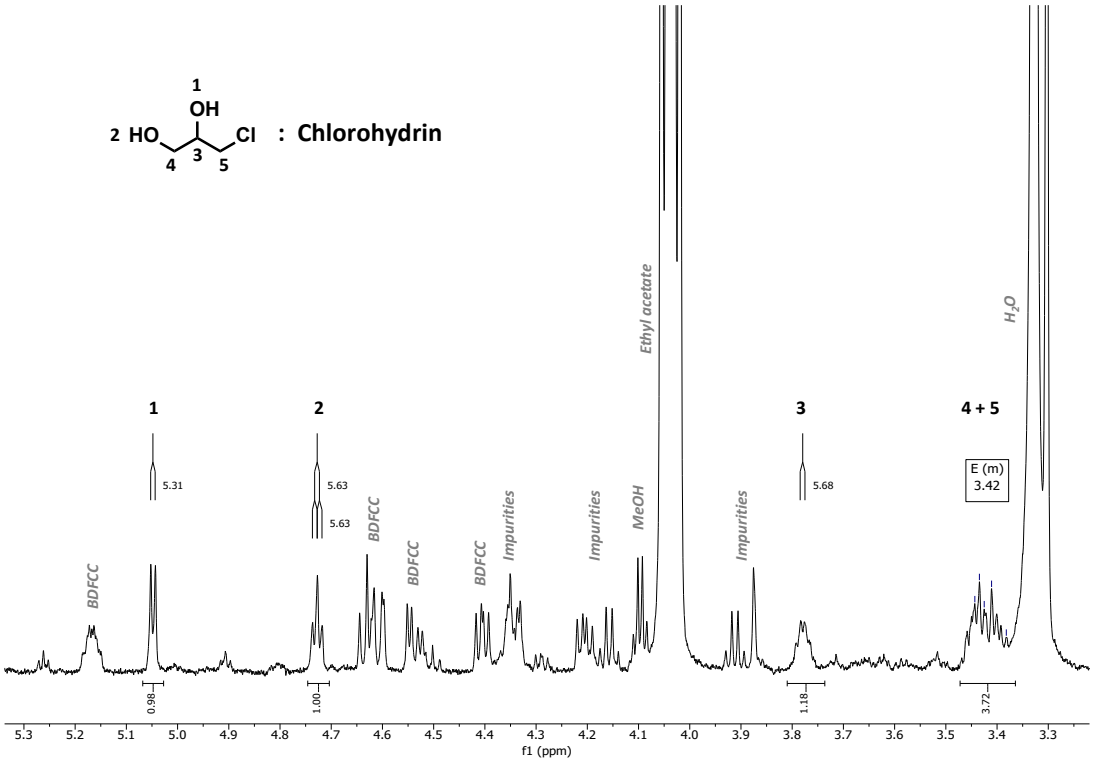

Figure S15 ^{1}H-NMR spectrum of FR5, highlighting the formation of chlorohydrin.

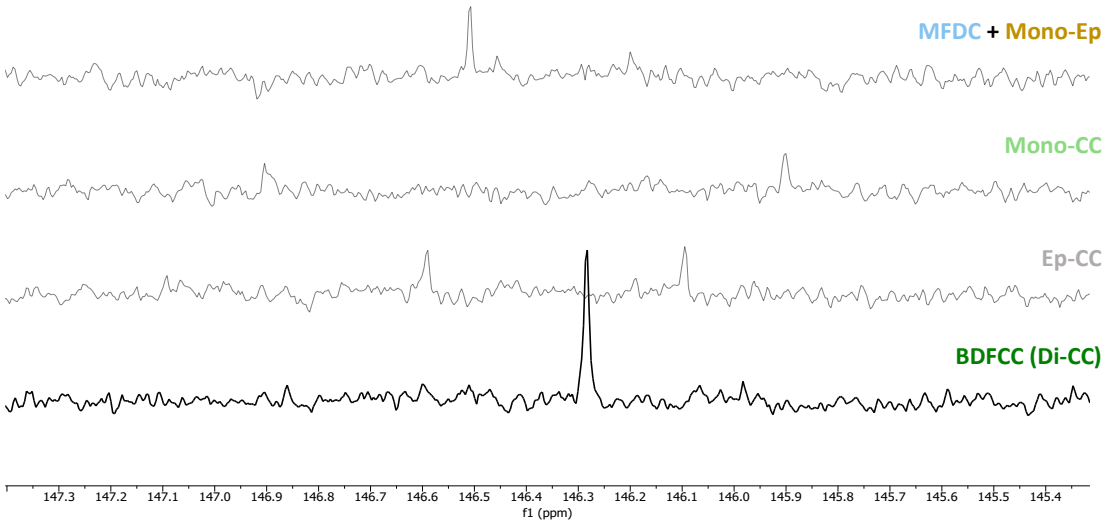

Figure S16 Stacked ^{13}C-NMR spectra of FR1-FR4: zoom at the 2,5-furanic carbon peaks.

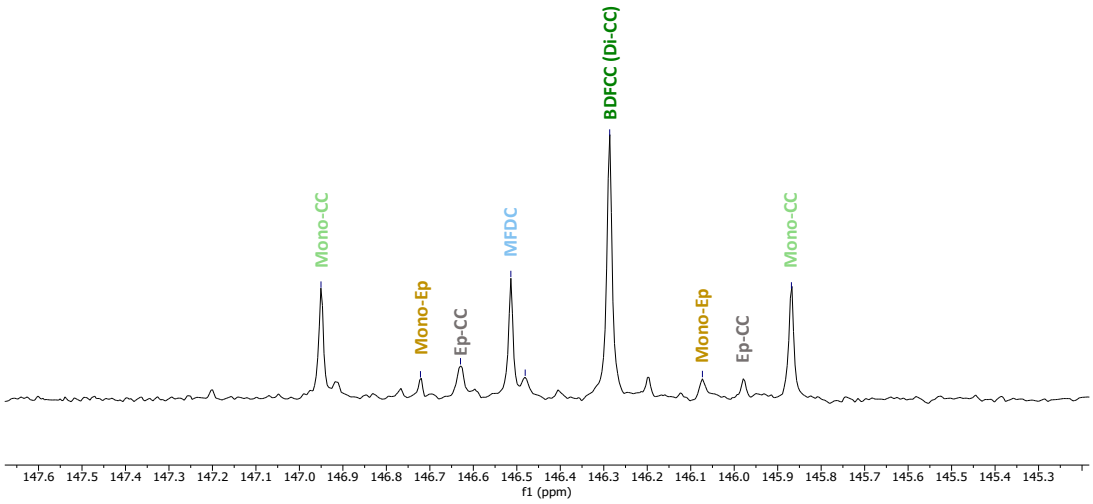

Figure S17 Representative ^{13}C-NMR spectrum of the crude reaction mixture: zoom at the quaternary furanic peaks.

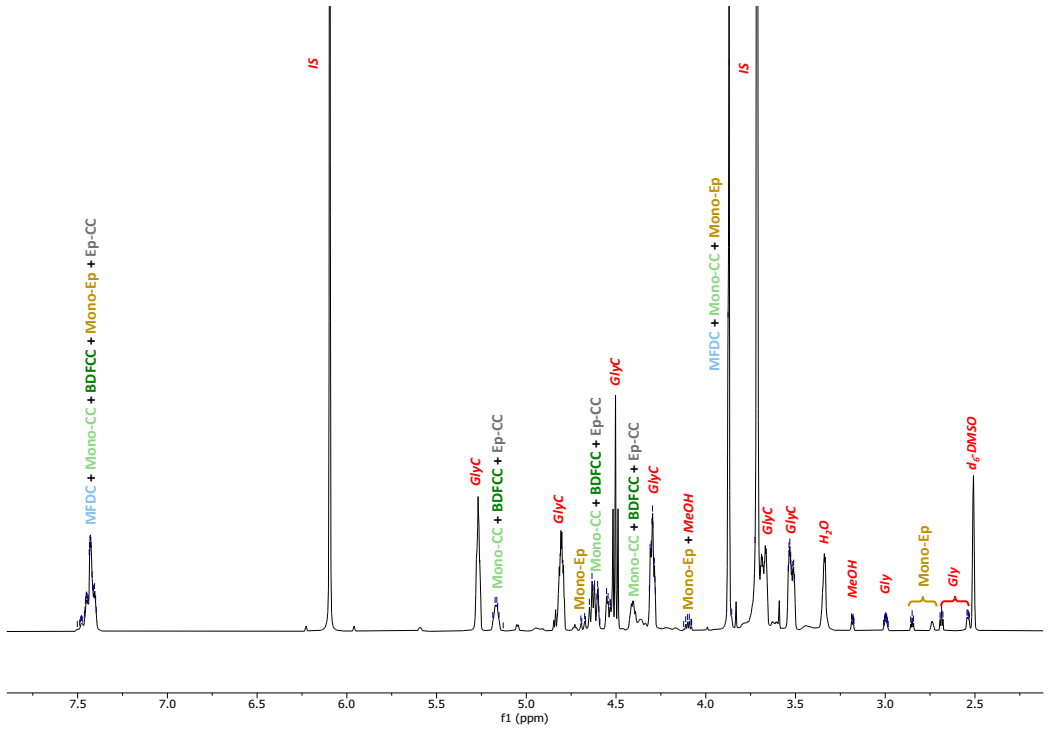

Figure S18 Representative ^{1}H-NMR spectrum of the crude reaction mixture.

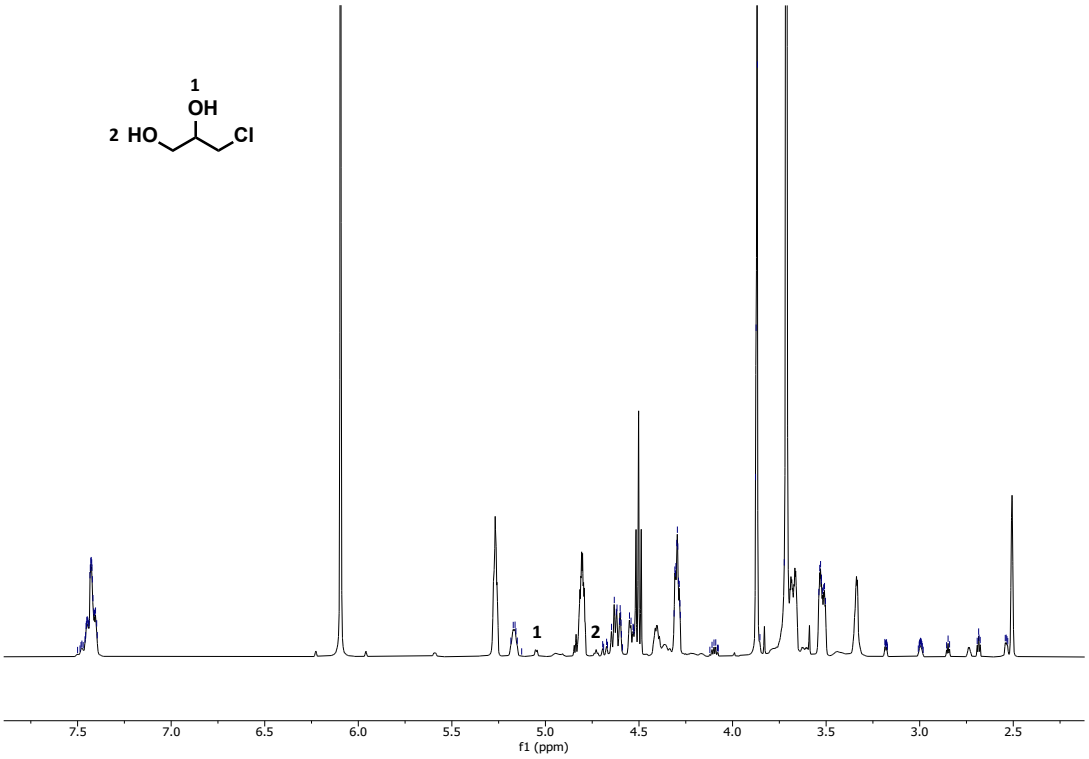

Figure S19 Chlorohydrin -OH peaks in the representative ^{1}H-NMR spectrum of the crude reaction mixture.

FT-IR spectra of reactants and products

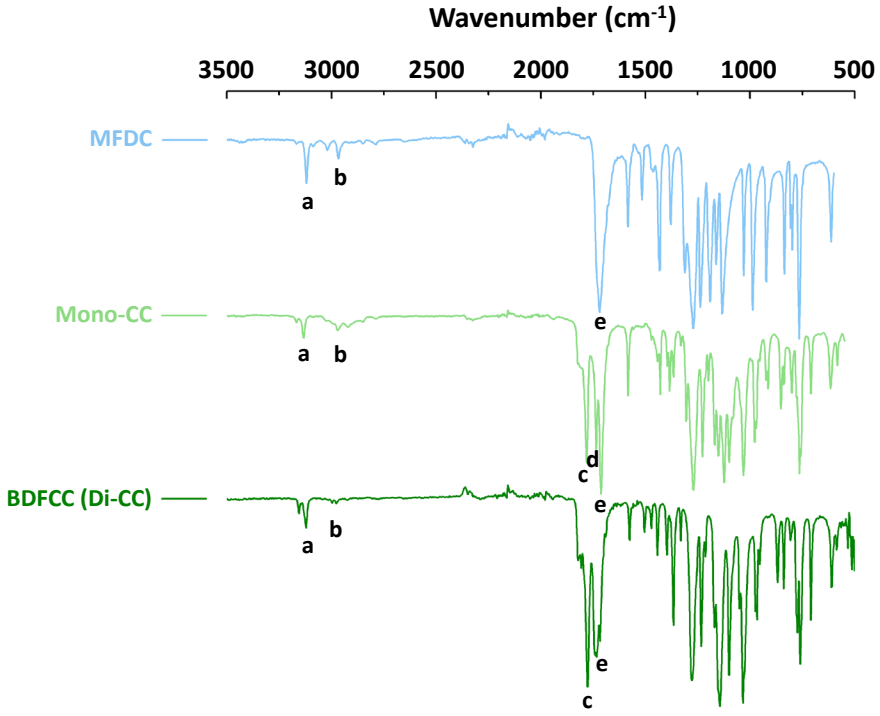

Figure S20 FT-IR spectrum of MFDC, Mono-CC and BDFCC (BDFCC). FT-IR signals (cm^{-1}): (a) 3118 (=CH, furanic ring), (b) 2964 (C-H), (c) 1782 (C=O, cyclic carbonate), (d) 1735 (C=O, ester), (e) 1719 (C=O, ester).

Catalyst characterisation by FT-IR spectroscopy

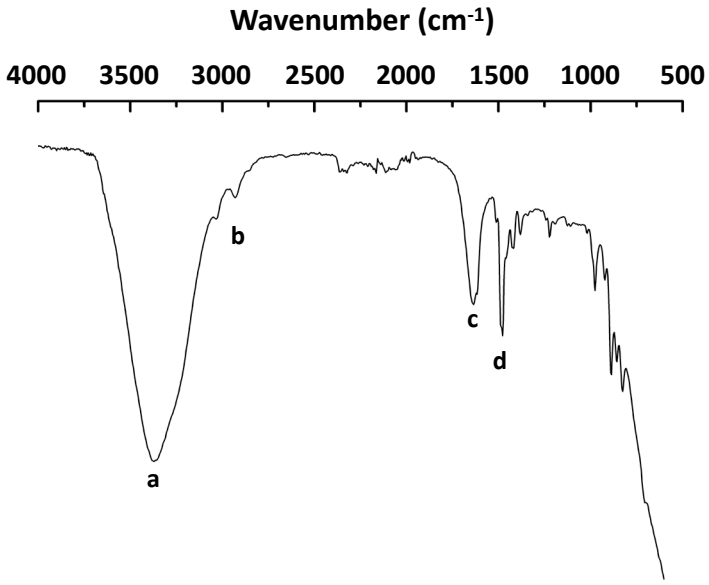

Figure S21 FT-IR spectrum of Amberlite IRA-900-Cl. Characteristic FT-IR signals (cm^{-1}): (a) 3350 (-OH from absorbed H_2O), (b) 3000 (C-H alkyl groups), (c) 1700 (C=C aromatic groups), (d) 1500 (quaternary ammonium groups and C-C aromatic groups).

Catalyst characterisation by scanning electronic microscopy (SEM)

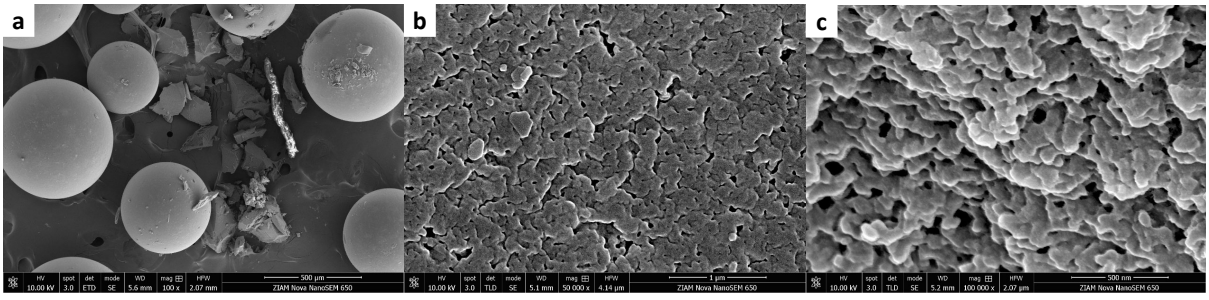

Figure S22 Scanning electron miscopy (SEM) analysis of Amberlite IRA-900-Cl resin beads at different magnifications: (a) Scale bar: 500 µm, magnification: 100 x; (b) Scale bar: 1 µm, magnification: 50 000 x; (c) Scale bar: 500 nm; magnification: 100 000 x.

Catalyst characterisation by thermogravimetric analysis (TGA)

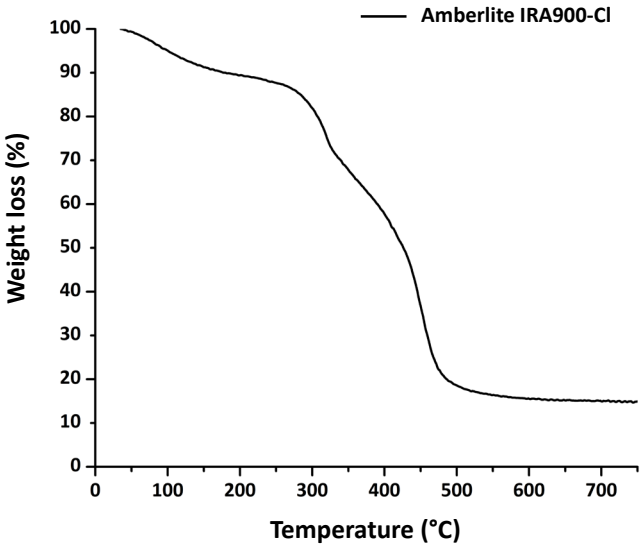

Figure S23 Thermogravimetric analysis (TGA) of Amberlite IRA-900-Cl resin beads**.** The initial weight loss starting at 30 °C is related to removal of physisorbed water, while the weight loss above 200 °C is attributed to polymer degradation.

References

1. https://chemicalsafety.ilo.org/dyn/icsc/showcard.listcards3?p_lang=en

2. Y. A. Alassmy, Z. Asgar Pour, and P. P. Pescarmona, *ACS Sustain. Chem. Eng.*, vol. 8, no. 21, pp. 7993–8003.